Supplementary Information

Crystal facet tailoring: a promising pathway toward high-performance $Y_{2/3}Cu_3Ti_4O_{12}$ thermosensitive ceramics

Yaxin Wei[a,b], Wenyuan Li[a,c], Jia Chen[a,c], Jianan Xu[a,c], Kai Li[d], Hanao Deng[a], Ke Zhao[b], Yahong Xie[b], Aimin Chang[a], Bo Zhang[a,*]

[a] *State Key Laboratory of Functional Materials and Devices for Special Environmental Conditions; Xinjiang Key Laboratory of Electronic Information Materials and Devices; Xinjiang Technical Institute of Physics & Chemistry of CAS, Urumqi, 830011, China*

[b] *Key Laboratory of Oil & Gas Fine Chemicals, Ministry of Education and Xinjiang Uyghur Autonomous Region, State Key Laboratory of Chemistry and Utilization of Carbon Based Energy Resources, College of Chemical Engineering and Technology, Xinjiang University, Urumqi, 830017, PR China*

[c] *Center of Materials Science and Optoelectronics Engineering, University of Chinese Academy of Sciences, Beijing, 100049, China*

[d] *Changchun Institute of Applied Chemistry of CAS, Changchun, 130022, China*

[*] *Corresponding author*

E-mail: zhangbocas@ms.xjb.ac.cn(Bo Zhang)

Experimental details

Preparation of precursors

The raw materials used for YCTO-*x*% oxide prepared by bioprotein method are as follows: deionized water (self-made in the laboratory), $Y(NO_3)_3 \cdot 6H_2O$ (purity≥ 99.0%; Aladdin), $Cu(NO_3)_2 \cdot 3H_2O$ (purity≥ 99.0%; Aladdin), Coconut water (commercially available), $Ti(OC_4H_9)_4$ (purity≥ 49.99%; Sinopharm), ethanol (AR) and bone glue (commercially available). Coconut water is not treated except by suction filtration.

Synthesis of Samples

The bioprotein method process is as follows: Mix bone glue with ethanol solution in a 1: 4 ratios to obtain a bone glue solution. $Y(NO_3)_3 \cdot 6H_2O$ and $Cu(NO_3)_2 \cdot 3H_2O$ were mixed into the ethanol solution in stoichiometric ratio to obtain the mixed solution I. $Ti(OC_4H_9)_4$ was added dropwise to the phase ethanol solution according to the stoichiometric ratio to form the mixed solution II. The solution I and II were mixed and stirred continuously to obtain solution III. Solution IV was obtained by mixing deionized water and coconut water in the ratios of 100%: 0%, 75%: 25%, 50%:5 0%, 25%: 75%, 100%: 0% and 125%: 0%, respectively. Coconut water is obtained by uniformly mixing multiple coconuts to eliminate individual differences between them. Solution IV, bone gum solution and solution III were homogeneously mixed on a constant temperature magnetic stirrer at 105°C in a molar ratio of 1.6: 1.6: 1 until a blue colloid was formed. Subsequently, the blue colloid matured at room temperature for 5 hours. After maturing, the blue gel is placed in a drying oven at 120℃ and dried for 48

hours to obtain honeycomb-like dry gel. To eliminate colloid, calcine the dry gel at 830–860°C to obtain YCTO-*x*% powder. The samples of YCTO obtained were named as YCTO-0%, YCTO-25%, YCTO-50%, YCTO-75%, YCTO-100%, and YCTO-125% according to the percentage of coconut water.

The YCTO-*x*% powder was pressed into disk with a radius of 5 mm using a uniaxial press at a pressure of 15 MPa. The cold isostatic press was adjusted to 280 MPa to further increase the density of the raw material. The YCTO-*x*% ceramics were finally obtained by holding in a chamber furnace at 940°C for 6 hours. Fig. 1 shows a simple process flow diagram of the bioprotein method.

Characterization of samples

The laser particle size analyzer (Malvern Mastersizer 3000, UK) is used to measure the particle size distribution of YCTO powders. Simultaneous thermal analysis of the dry gels was obtained by thermogravimetric analysis and differential scanning calorimetry (TG/DSC; NETZSCH STA449F, Germany) at a heating rate of 10°C/min. X-ray diffraction (XRD; BRUKER D8-ADVANCE, Germany) was used to obtain the phase structure of the samples by Cu-Ka irradiation (λ=1.5406 Å, 40 mA and 40 kV). Diffraction spectra in the range of 10°–80° at room temperature were collected when the step size was 0.02° and the counting time was 0.2 s/step. High-precision XRD data were obtained using the step scan mode. Scanning electron microscopy (SEM; Zeiss SUPRA 55 VP, Germany) was used to measure the morphology of the samples and to image the YCTO-B cross-section. The average grain size of YCTO ceramics was

predicted by Nano Measurer 1.2 software using the intercept method. In order to facilitate the visualization of cubic grains, the cutting of the sample was done by focused ion beam scanning electron microscopy (FIB; Helios 5 cx, Czech Republic) with a Ga ion beam. The crystallographic information of the thin sections was obtained by transmission electron microscopy (HRTEM; JEM-F200, JEOL) at an accelerating voltage of 200 kV. The strain results from HRTEM were calculated using the commercial Geometric Phase Analysis (GPA) package. A U-3900 UV-vis spectrophotometer (U-3900, Hitach, Japan) was used to acquire the UV-vis transmission spectra. The elemental chemical valence states of the ceramic samples were obtained by X-ray photoelectron spectroscopy (XPS; ESCALAB 250XI, Thermo).

Electrical property measurements

For electrical properties, a thin layer of silver paste was applied to both sides of the ceramics and then annealed at 710°C for 45 minutes. The resistance of the samples was measured in the temperature range of 25–600°C using a digital multimeter. Aging experiments were performed in a 200°C drying oven and resistance data was obtained every 100 hours. The aging coefficient is calculated by the following equation: $\Delta R/R_0 = [|R_x - R_0| /R_0] \times 100\%$, Where ΔR is the absolute value of the difference between the resistance before R_0 is the resistance of the unaged sample at 200°C and after aging and R_x is the resistance at 200°C after aging for x hours.

Computational details

All calculations were carried out within the framework of density functional theory using the projection enhanced plane wave method and implemented in the Vienna ab initio simulation package (VASP)[1] We used the Generalized Gradient Approximation (GGA) with Pedrew-Burke-Ernzerhof (PBE) function[2]. The cut-off energy of the plane wave is set to 500 eV. When iteratively solving the Kohn Sham equation, the energy standard is set to 10^{-5} eV. To avoid artificial interactions between periodic images, a 15 Å vacuum layer was added perpendicular to the thin film. Brillouin zone integration using a 3x3x1 k grid. All structures were relaxed until the residual force on the atoms decreased to less than 0.01 eV/Å.

The surface models of the {100}, {110} and {111} faces are constructed on the basis of the slab model with the same thickness of the vacuum region as that of the YCTO crystal. In addition, each surface is cut to create a non-polar surface. Atomic stoichiometry is met on each side of the slab. Geometric relaxation with mid-layer fixation. All surfaces are calculated using the (1×1) periodic slab model, with symmetric adsorption on both sides of the slab. All atoms are relaxed without any constraints. A cutoff of E_{cut} = 450 eV was used for the plane-wave basis set. In the case of slab, the vacuum space is greater than 15 Å. Calculate surface energy using the following formula (γ)：

$$\gamma = \frac{E_{slab} - nE_{bulk}}{2A},$$

where E_{slab} is the total energy of the slab, E_{bulk} is the total energy of the bulk of each cell, n is the number of bulk cells contained in the slab, and A is the surface area

of each side of the slab.

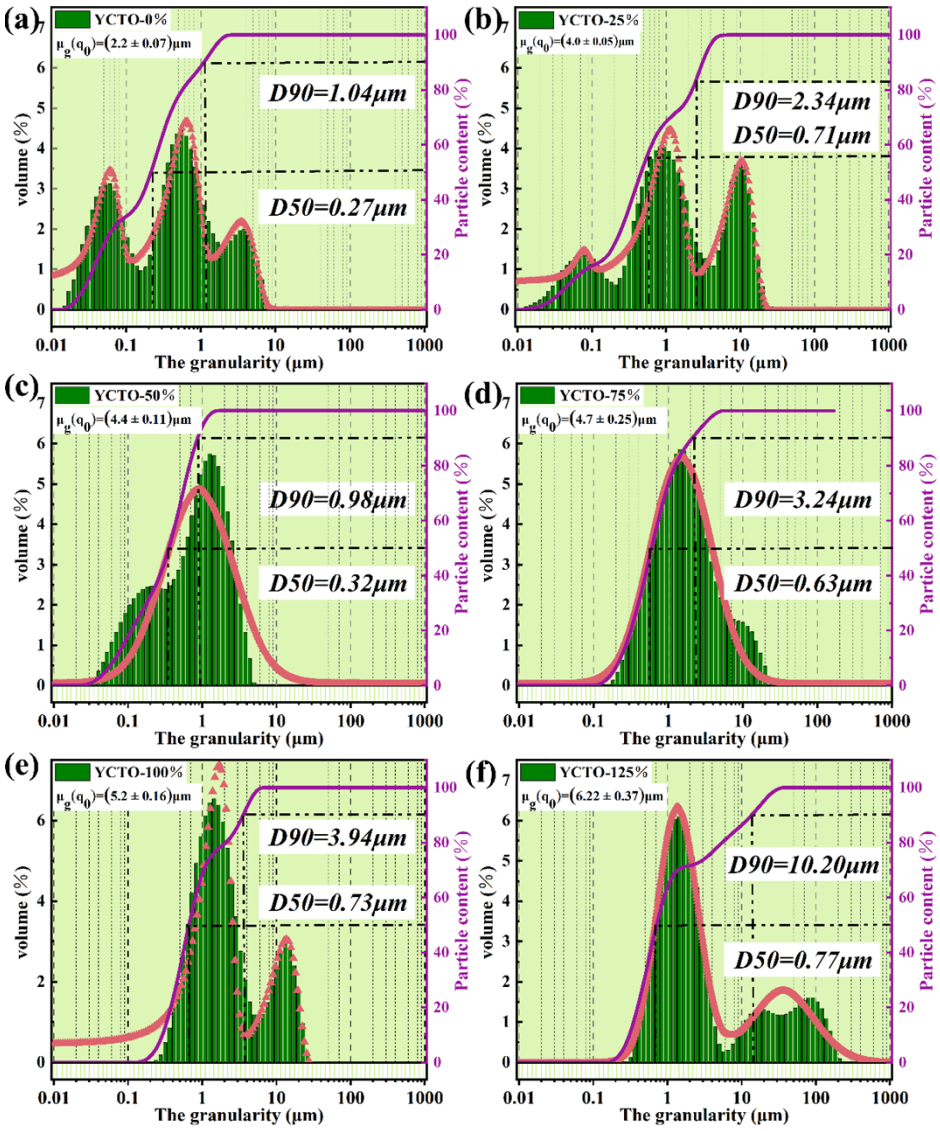

Fig. S1. Particle size distribution of YCTO-*x*% powders.

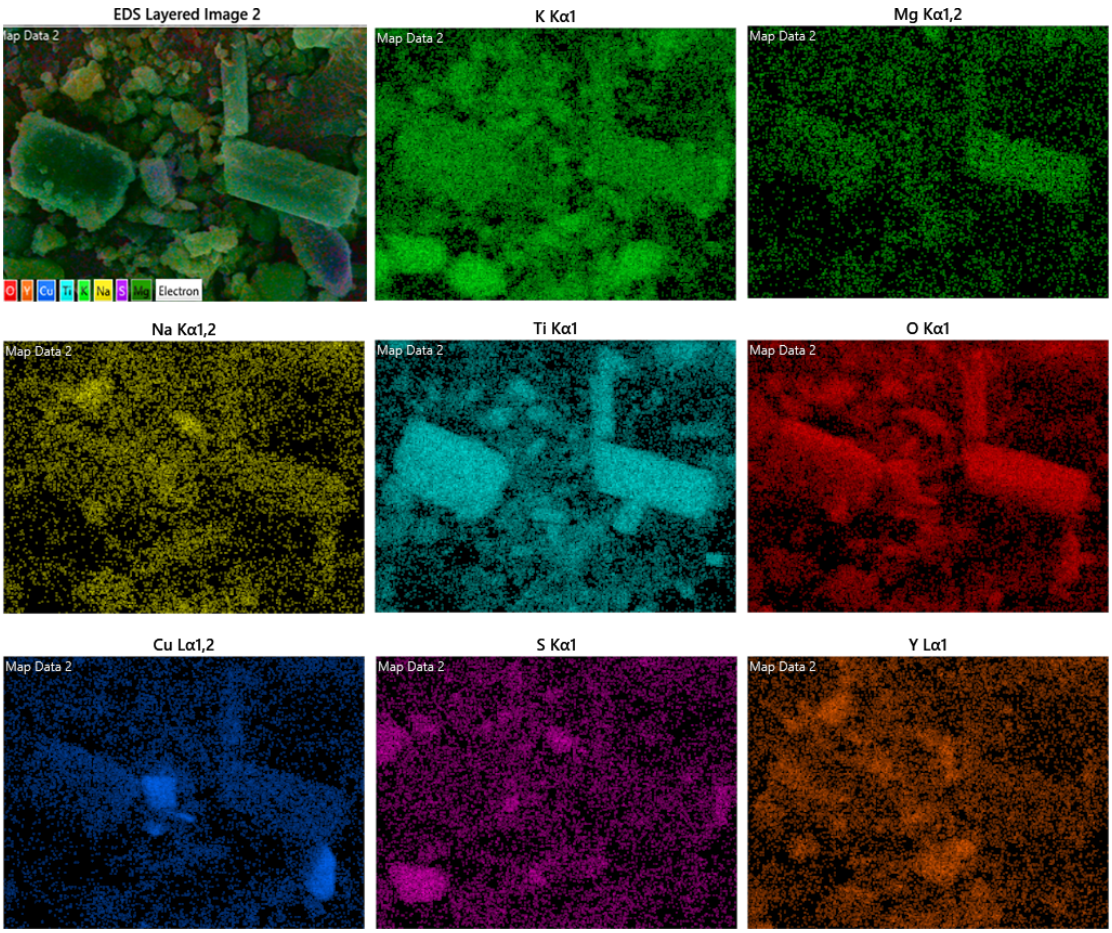

Fig. S2. Element mapping of rod-shaped particles in YCTO-125% powder.

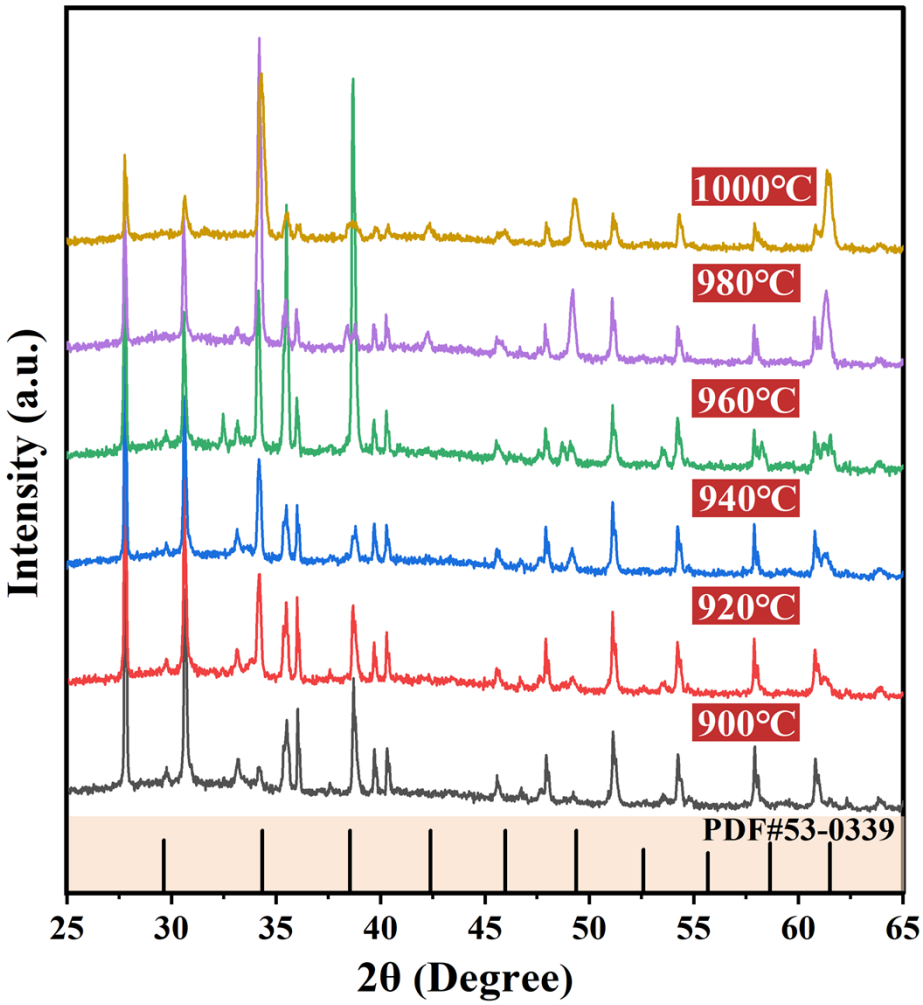

Fig. S3. X-ray diffraction (XRD) patterns of YCTO-125% ceramics were obtained after annealing at 900℃, 920℃, 940℃, 960℃, 980℃, and 1000℃, respectively.

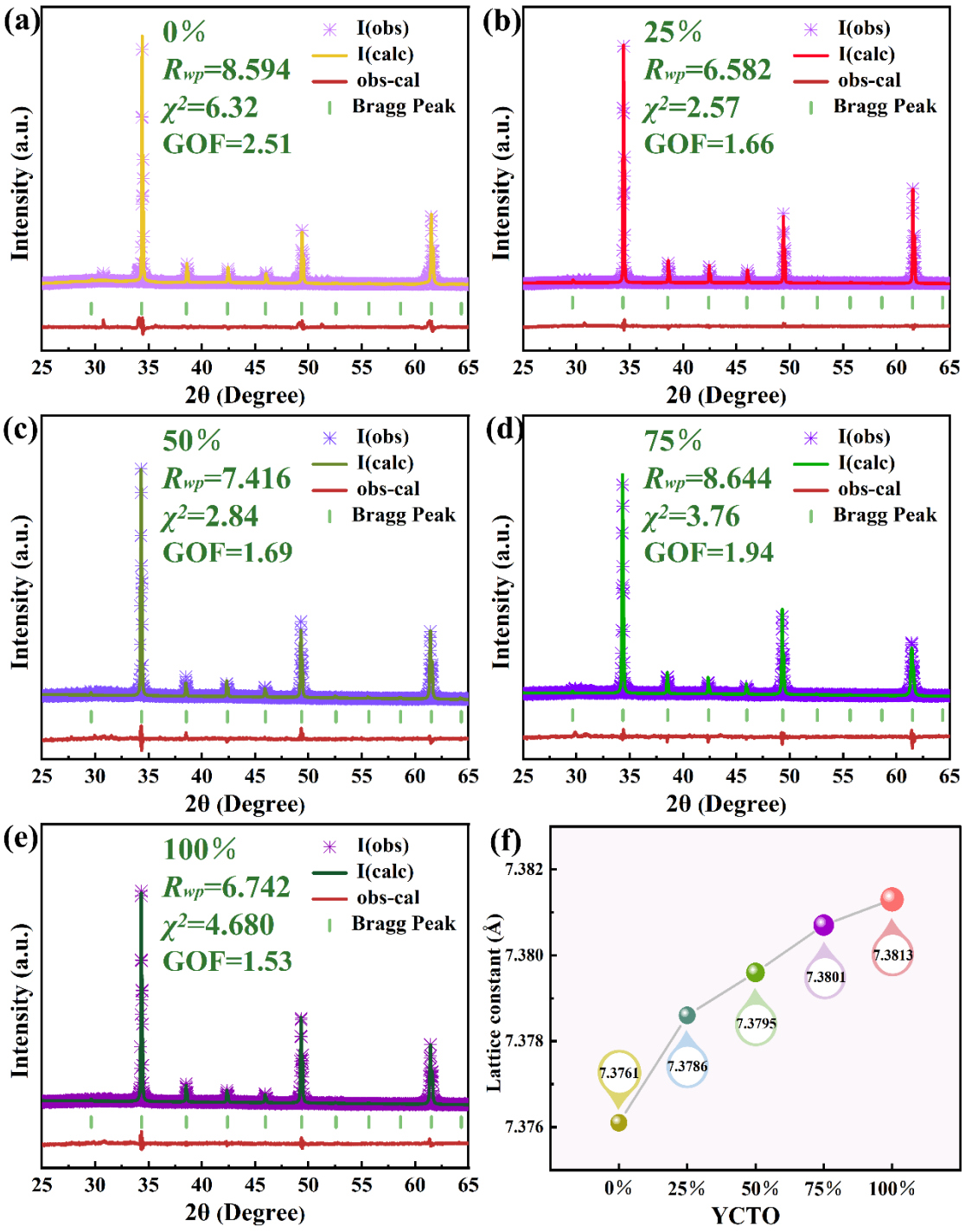

Fig. S4. (a-e) Rietveld fitting of XRD patterns of YCTO-*x*% ceramics; (f) The lattice parameters of YCTO-*x*% ceramics obtained after Rietveld refinement of XRD.

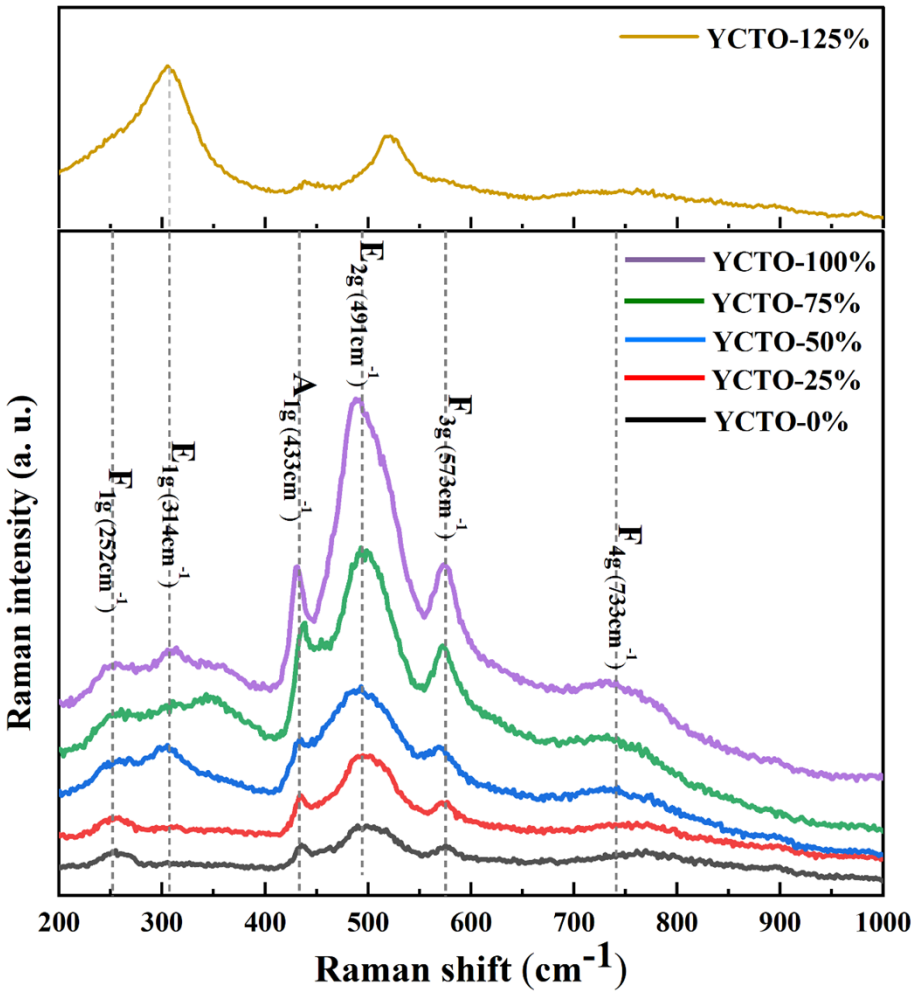

Fig. S5. Raman curves of YCTO-*x*% ceramics.

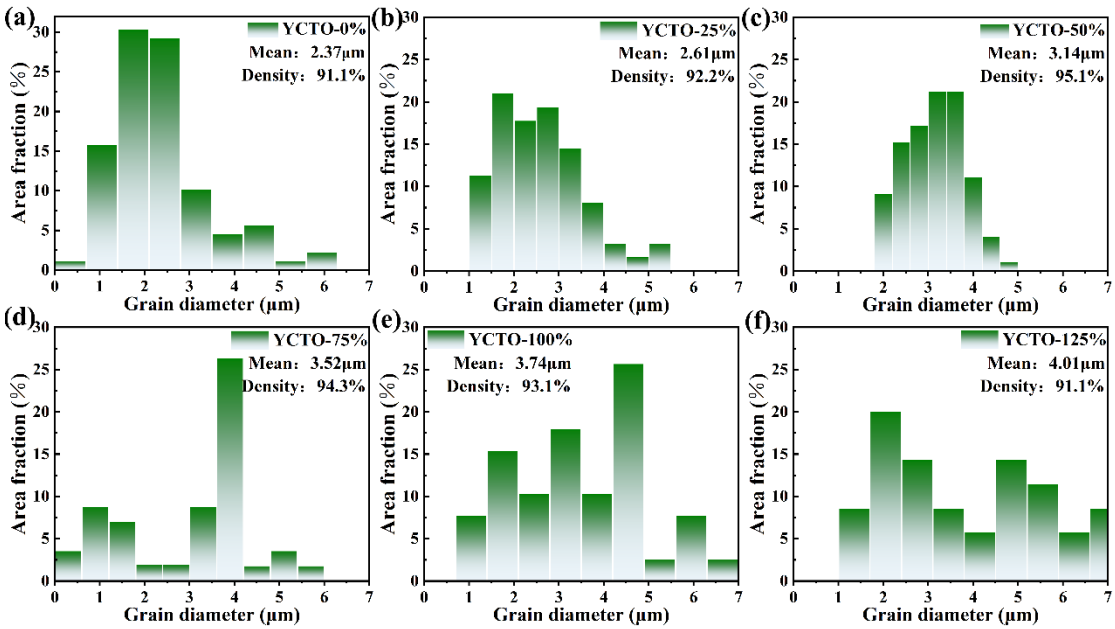

Fig. S6. (a-f) Particle size distribution of YCTO-*x*% (*x*=0%, 25%, 50%, 75%, 100%, 125%) ceramic grains.

Table S1. Atomic percentages and the molar ratio of elements in YCTO-*x*% ceramics.

Sample	Atomic percentages of elements (at. %)								Molar ratio
	$Y_{2/3}$	Cu	Ti	O	K	Na	Mg	S	$Y_{2/3}$: Cu: Ti: O: "impurity ion"
YCTO-0%	3.41	15.30	20.12	61.15	\	\	\	\	0.67: 2.99: 3.94: 11.99: 0
YCTO-25%	3.15	18.79	19.90	58.16	\	\	\	\	0.66: 3.93: 4.17: 12.18: 0
YCTO-50%	3.41	15.04	19.86	61.15	0.52	\	\	\	0.67: 2.95: 3.89: 11.99: 0.10
YCTO-75%	3.44	15.03	19.16	61.46	0.88	\	\	\	0.65: 2.98: 3.79: 2.17: 0.17
YCTO-100%	3.40	14.70	18.46	61.95	0.89	0.43	0.17	\	0.68: 2.94: 3.50: 12.39: 0.29
YCTO-125%	3.28	15.24	19.40	60.05	0.95	0.56	0.27	0.19	0.67: 2.99: 3.96: 11.97: 0.41

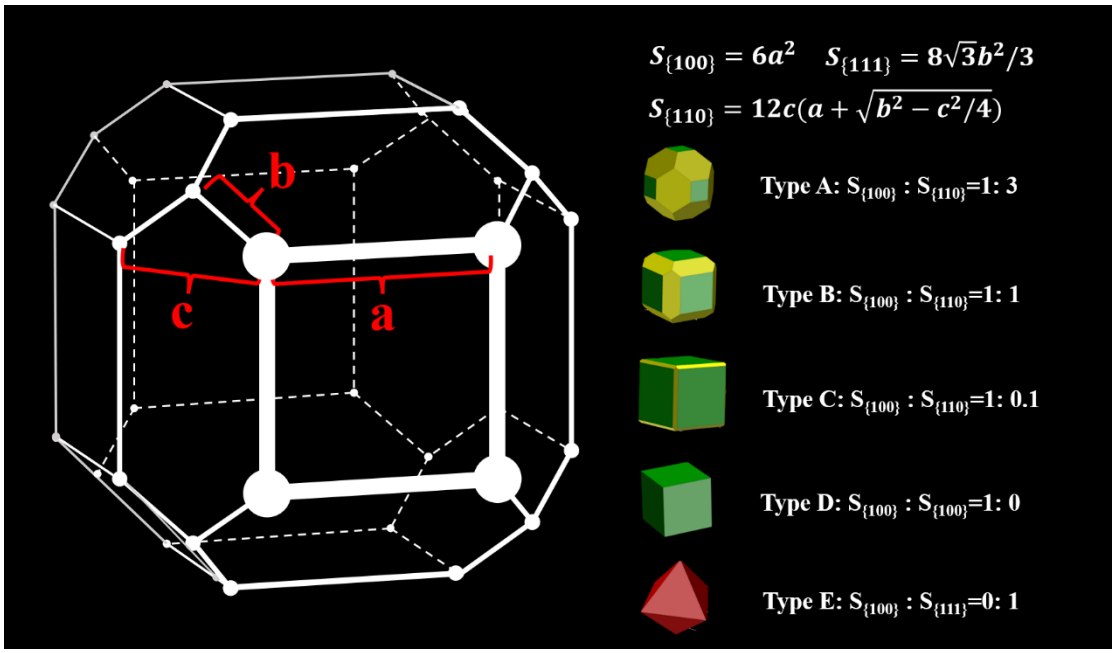

Fig. S7. Calculations of the percentage of {100} facets and {110} facets. Type A crystals are cubes with six {100} facets. Type B, C, D are 18-hedrons with six {100} facets and twelve {110} facets. From type A to type D, the ratio of {110} facets to {100} facets increase. Type E crystals are octahedral with eight {111} facets. Note that these numbers are simple estimates.

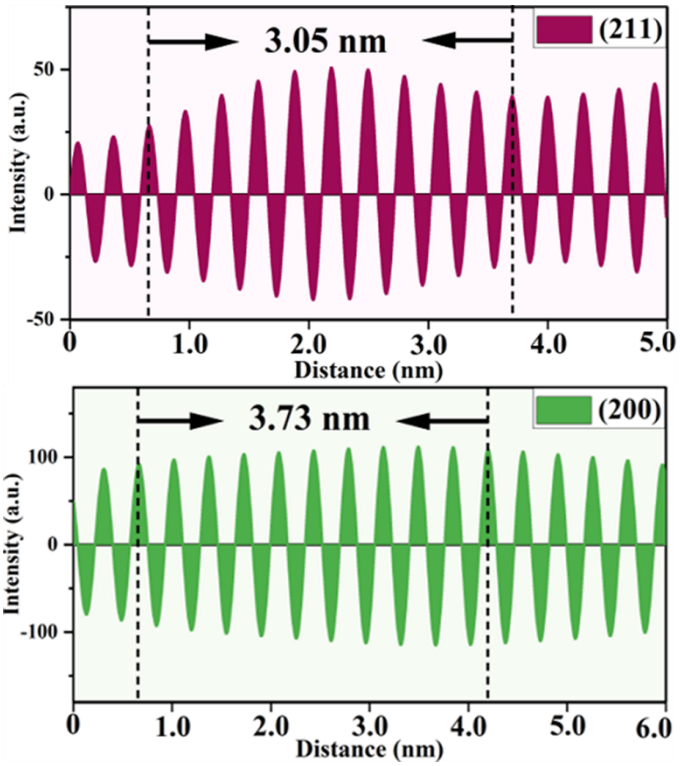

Fig. S8. The distribution of atomic intensity curves of Fig. 6b.

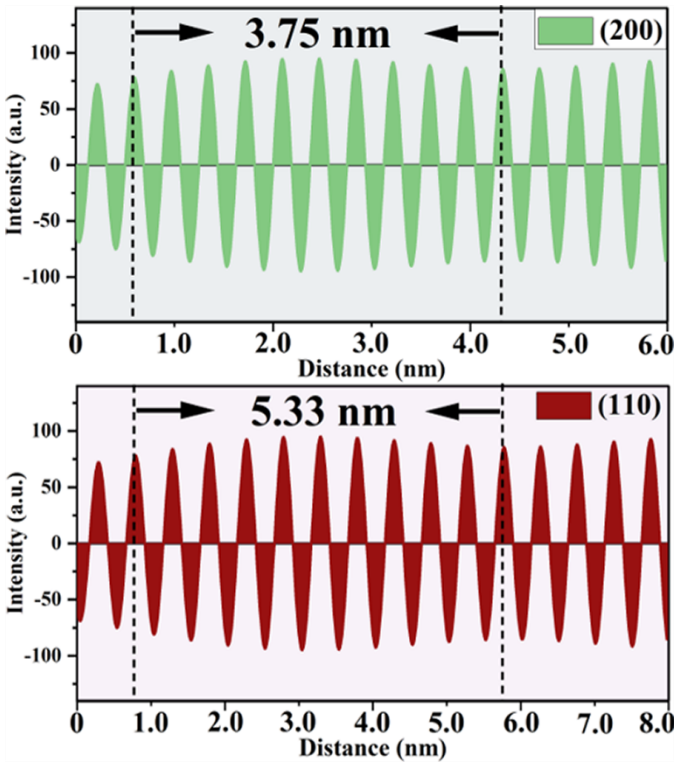

Fig. S9. The distribution of atomic intensity curves of Fig. 6i.

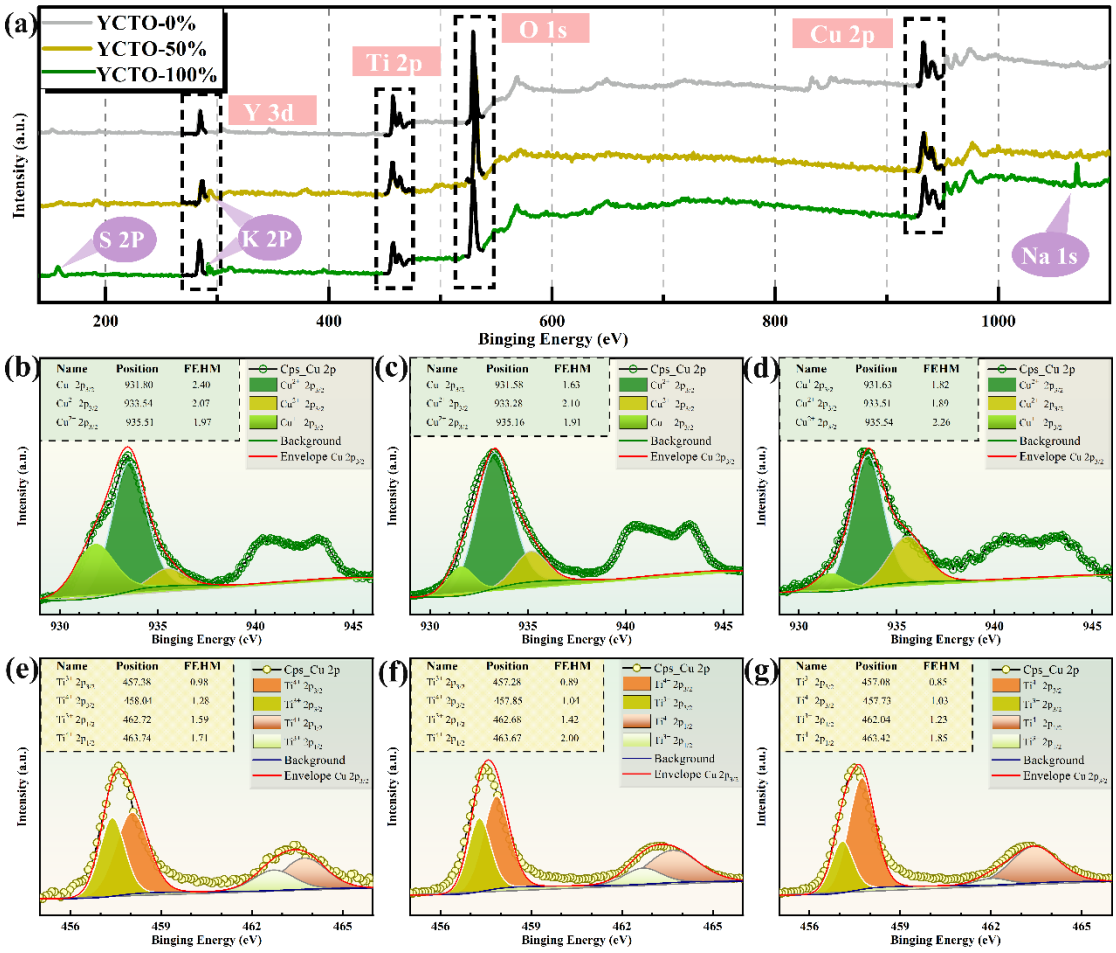

Fig. S10. (a) XPS full spectrum of YCTO-0%, YCTO-50% and YCTO-100% ceramics. XPS fitted spectrum of individual elements of YCTO-0%, YCTO-50% and YCTO-100% ceramics: (b-d) Cu 2p regions, (e-g) Ti 2p regions.

To further obtain the changes in chemical composition and ionic valence states due to different crystal faces. Therefore, quantitative analysis of YCTO ceramic surfaces with 0%, 50% and 100% coconut water were carried out using XPS. Fig. S11(a) shows the full XPS spectrum corrected using the C 1s peak (binding energy of 284.91 eV) to balance the deviation of the spectrum caused by the charge effect. Through peak searching of the entire spectrum, it was found that except for the Auger peaks corresponding to Y, Cu, Ti, and O, no other elements were found in YCTO-0%. This is consistent with the EDS analysis results, confirming the purity of the elements

in the sample. In addition to the elements in the design, Na, K, Mg and S elements were also identified in ceramics containing coconut water. This confirms the presence of coconut water residue and forms a good chemical reaction in the solid solution. The XPS patterns confirm the spin splitting in YCTO ceramics from the $2p_{3/2}$ orbital of Cu elements and the $2p_{1/2}$ and $2p_{3/2}$ orbitals of Ti elements. This result is consistent with previous studies. The contributions corresponding to Cu^{2+}/Cu^{+} (Fig. S11b-d) and Ti^{4+}/Ti^{3+} (Fig. S11e-g) on the 2p orbitals of Cu and Ti, were confirmed using Gauss-Lorentz function curve fitting. The binding energies of their Cu^{+}, Cu^{2+}, Ti^{3+} and Ti^{4+} auger peaks lie in the ranges of 934.39–934.90 eV, 931.58–933.56 eV, 457.58–463.84 eV and 457.07–462.95 eV, respectively. Quantitative data are presented in Table S2.

Table S2. The concentration of Cu^{+} and Ti^{3+}, and the ionic ratios of Ti^{3+}/Ti^{4+} and Cu^{+}/Cu^{2+}.

Sample	Ionic ratio of Cu^{+}/Cu^{2+}	Ionic ratio of Ti^{3+}/Ti^{4+}	Concentration of Cu^{+} (at. %)	Concentration of Ti^{3+} (at. %)	O_L concentration (at. %)
YCTO-0%	0.42	0.69	29.83	40.95	54.99
YCTO-50%	0.13	0.54	11.90	35.39	75.49
YCTO-100%	0.08	0.27	8.40	21.69	85.21

Table S3. Comparison of aging parameters of NTC thermistors.

Investigators	Chemical compositions	Aging time	Aging temperature	*ΔR/R*
Li et al.[1]	$Mn_{2.15}Cu_{0.4}Ni_{0.45}O_4$	800 h	125°C	22.5%
Xia et al.[2]	$Mn_{1.05-y}Co_{1.95-x-z-w}Ni_xMg_yAl_zFe_wO_4$	600 h	910°C	less than 10%
Balitska et al.[3]	$Cu_{0.1}Ni_{0.8}Co_{0.2}Mn_{1.9}O_4$	1000 h	125°C	4
Vakiv et al.[4]	$Cu_{0.1}Ni_{0.8}Co_{0.2}Mn_{1.9}O_4$	170 h	500°C	3.5%
Zhao et al.[5]	$Cu_xZn_{1.0}Ni_{0.5}Mn_{1.5-x}O_4$	1000 h	150°C	less than 2.6%
Liu et al.[6]	$CaMn_{0.05}Zr_{0.95}O_{3-x}$-$NiMn_2O_4$ (x=0, 0.1, 0.2, 0.3)	150 h	900°C	2.1%
Fu et al.[7]	$0.3CaCeNbWO_8$-$0.7LaMnO_3$	200 h	300°C	less than 2%
Teichmann et al.[8]	$Zn_{0.5}Ni_{0.5}Co_{0.5}Mn_{1.5-x}Cu_xO_4$ ($0.1 \le x \le 0.4$)	600 h	150°C	2%
Liu et al.[29]	$Ca_{0.9}R_{0.1}CeNbMoO_8$ (R = Y, Sm, Nd, La)	200 h	800°C	less than 2%
Gao et al.[10]	$(Zn_{0.4}Ni_{0.6})_{1-x}Na_xO$ (xZNN, x< 0.1)	170 h	150°C	1.8%
Ren et al.[11]	$Zn_{0.4}Fe_{2.1}Co_2Mn_{1.5}O_8$	125 h	500°C	1.02%
Fang et al.[12]	$Fe_xCu_{0.10}Ni_{0.66}Mn_{2.24-x}O_4$	500h	150°C	0.60%
Guan et al.[13]	$LaMn_{0.3}Ti_{0.7}O_3$-$NiMn_2O_4$	1000 h	125°C	0.52%
Fang et al.[14]	$Ni_xMn_{3-x}O_{4+\delta}$ ($0.56 \le x \le 1.0$)	1000 h	150°C	0.5%
Varghese et al.[15]	$Ni_{0.75}Mn_{(2.25-x-y)}Cr_xFe_yO_4$; x = 0.05–0.25, y = 0, 0.05, 0.25	168 h	150°C	0.5%
Hao et al.[16]	$Co_{1.7}Ni_{1.3-x}Al_xO_4$ ($0 \le x \le 0.5$)	500 h	125°C	0.32%
This work	YCTO-50%	1000 h	200°C	0.1%

References

[1] D.-F. Li, S.-X. Zhao, K. Xiong, H.-Q. Bao, C.-W. Nan, Aging improvement in Cu-containing NTC ceramics prepared by co-precipitation method, Journal of Alloys and Compounds 582 (2014) 283–288. https://doi.org/10.1016/j.jallcom.2013.08.014.

[2] J. Xia, Q. Zhao, B. Gao, A. Chang, B. Zhang, R. Ma, Preparation and electrical properties of $Mn_{1.05-y}Co_{1.95-x-z-w}Ni_xMg_yAl_zFe_wO_4$ NTC ceramic derived from microemulsion method, Journal of Alloys and Compounds 591 (2014) 207–212. https://doi.org/10.1016/j.jallcom.2013.12.021.

[3] V.O. Balitska, B. Butkievich, O.I. Shpotyuk, M.M. Vakiv, On the analytical description of ageing kinetics in ceramic manganite-based NTC thermistors, Microelectronics Reliability 42 (2002) 2003–2007. https://doi.org/10.1016/S0026-2714(02)00096-3.

[4] M.M. Vakiv, O.I. Shpotyuk, V.O. Balitska, B. Butkiewicz, L.I. Shpotyuk, Ageing behavior of electrical resistance in manganite NTC ceramics, Journal of the European Ceramic Society 24 (2004) 1243–1246. https://doi.org/10.1016/S0955-2219(03)00377-7.

[5] C. Zhao, B. Wang, P. Yang, L. Winnubst, C. Chen, Effects of Cu and Zn co-doping on the electrical properties of $Ni_{0.5}Mn_{2.5}O_4$ NTC ceramics, Journal of the European Ceramic Society 28 (2008) 35–40. https://doi.org/10.1016/j.jeurceramsoc.2007.06.007.

[6] Y. Liu, W. Deng, X. Chen, Y. Xue, X. Bai, H. Zhang, A. Chang, Y. Xie,

$CaMn_{0.05}Zr_{0.95}O_3$–$NiMn_2O_4$ composite ceramics with tunable electrical properties for high temperature NTC thermistors, Ceramics International 48 (2022) 33455–33461. https://doi.org/10.1016/j.ceramint.2022.07.289.

[7] Z. Fu, Y. Liu, B. Zhang, A. Chang, Highly dense $0.3CaCeNbWO_8$ -$0.7LaMnO_3$ composite ceramics fabricated by cold sintering process, J Am Ceram Soc 103 (2020) 6586–6593. https://doi.org/10.1111/jace.17353.

[8] C. Teichmann, J. Töpfer, Sintering and electrical properties of Cu-substituted Zn-Co-Ni-Mn spinel ceramics for NTC thermistors thick films, Journal of the European Ceramic Society 42 (2022) 2261–2267. https://doi.org/10.1016/j.jeurceramsoc.2021.12.078.

[9] Y. Liu, Z. Fu, X. Chen, Y. Wei, B. Zhang, A. Chang, Microstructural and electrical changes in $Ca_{0.9}R_{0.1}CeNbMoO_8$ (*R*=Y, Sm, Nd, La) ceramics induced by rare-earth ion doping, J. Am. Ceram. Soc. 104 (2021) 2134–2142. https://doi.org/10.1111/jace.17670.

[10] C. Gao, Z. Li, L. Yang, D. Peng, H. Zhang, Investigation of electrical and aging properties of Bi-modified $(Zn_{0.4}Ni_{0.6})_{1-x}Na_xO$ ceramic thermistors, Journal of the European Ceramic Society 41 (2021) 4160–4166. https://doi.org/10.1016/j.jeurceramsoc.2021.02.030.

[11] W. Ren, N.-N. Zhu, L. Li, H.-J. Feng, Y.-G. Wang, Y.-H. Yang, Z.-N. Yang, S.-G. Shang, Improvement of ageing issue in $Zn_{0.4}Fe_{2.1}Co_2Mn_{1.5}O_8$ thermistor films, Journal of the European Ceramic Society 39 (2019) 4189–4193. https://doi.org/10.1016/j.jeurceramsoc.2019.05.068.

[12] D. Fang, C. Chen, A.J.A. Winnubst, Preparation and electrical properties of $Fe_xCu_{0.10}Ni_{0.66}Mn_{2.24-x}O_4$ ($0 \leq x \leq 0.90$) NTC ceramics, Journal of Alloys and Compounds 454 (2008) 286–291. https://doi.org/10.1016/j.jallcom.2006.12.059.

[13] F. Guan, X. Lin, H. Dai, J. Wang, X. Cheng, S. Huang, $LaMn_{1-x}Ti_xO_3$-$NiMn_2O_4$($0 \leq x \leq 0.7$): A composite NTC ceramic with controllable electrical property and high stability, Journal of the European Ceramic Society 39 (2019) 2692–2696. https://doi.org/10.1016/j.jeurceramsoc.2019.03.003.

[14] D. Fang, C. Zheng, C. Chen, A.J.A. Winnubst, Aging of nickel manganite NTC ceramics, J Electroceram 22 (2009) 421–427. https://doi.org/10.1007/s10832-008-9467-5.

[15] J.M. Varghese, A. Seema, K.R. Dayas, Microstructural, electrical and reliability aspects of chromium doped Ni–Mn–Fe–O NTC thermistor materials, Materials Science and Engineering: B 149 (2008) 47–52. https://doi.org/10.1016/j.mseb.2007.12.005.

[16] H. Fu, W. Zhang, T. Zhou, Z. Wang, C. Chen, Preparation and Characterization of $Co_{1.7}Ni_{1.3-x}Al_xO_4$ ($0.1 \leq x \leq 0.5$) NTC Ceramics with Low B-Value and High Resistivity, J. Electron. Mater. 51 (2022) 4836–4845. https://doi.org/10.1007/s11664-022-09726-0.